RESPONSE OF A TIGHTLY CLUSTERED NUCLEAR FUEL ELEMENT BUNDLE TO ARBITRARY INITIAL THERMAL AND MECHANICAL LOADING CONDITIONS

A.J. BAUMGARTNER,

Atomics International, North American Rockwell, Canoga Park, California, U.S.A.

ABSTRACT

The mechanical response of nuclear fuel elements (thin-walled tubes) to their thermal environment is closely controlled by a system of mechanical constraints and support conditions. These two factors determine primarily the mechanical interactions between and relative deflections of the fuel elements. The relative deflection response, in general, modifies the initial (nominal) geometry of the coolant flow channels, and with it the associated temperature distribution in the flow channels. Finally, this new temperature distribution about the fuel elements replaces the initial nominal temperature environment. The solution to this problem requires determination of the steady-state relationship between all fuel element force-deflection responses, and the temperature distribution in all coolant flow channels. This situation clearly suggests a solution approach involving iterations, as indicated subsequently.

The initial phase of the method treats each element of the bundle on a noninteractive basis. A set of equations is developed to convert the arbitrary circumferential temperature distribution into an equivalent linear diametral thermal gradient. Next, the corresponding rotation of the end faces, including associated angular directions, is determined for each incremental element length.

A unique computer algorithm was developed to assemble these incremental beams into a continuous 3-dimensional "free-bow" shape for each fuel element. Placing each of the "free" elements into its designated location within the bundle sets the stage for studying the interactions between these elements.

The task of determining the inter-element force at points of interference is accomplished by an iterative scanning procedure. Each subsequent round of iteration modifies the initial set of interference forces to more closely result in a near-zero gap at the points of initial interference.

The last phase of the interference study procedure determines a modified set of initial thermal conditions compatible with the new coolant channel geometries, as defined

by the mechanical iteration results. Derivation of the new flow channel temperatures assumes that, at a given element channel nodal point, heat flow rates and axial coolant pressure gradients remain essentially unchanged from the initial conditions.

A new round of thermal iterations begins at this point, on the basis of the new thermal conditions. The acronym for the associated computer program is "SAS3D." It is written in FORTRAN IV and is operated on the IBM-360/65 or 360/85 System.

I. INTRODUCTION

The problem presented herein is encountered invariably in the structural optimization phase of fuel rod banks for a liquid metal cooled nuclear reactor. The "first cut" approach in dealing with this problem often consists of making numerous "worst case" assumptions. The attendant massive conservatism, when finally recognized, often renders this approach unacceptable, from a point of view of materials limitations. Alternatively, one may be tempted to "design around" the problem, by resorting to a series of preventative design measures compounding design complexity and sometimes redundant in purpose.

This paper presents a third and, generally, much more successful design alternate to the problem of predicting thermo-mechanical cause and effect relationships within a tightly clustered nuclear fuel element bundle. The approach presented here is the more valuable since it yields a multiply-iterated steady-state solution, thereby allowing to more closely approach the structural design limits of critical materials. The problem studied herein is very briefly described as follows:

The mechanical response of nuclear fuel elements (thin-walled tubes) to their thermal environment is closely controlled by a system of mechanical constraints and support conditions. These two factors determine primarily the mechanical interactions between and relative deflections of the fuel elements. The relative deflection response, in general, modifies the initial (nominal) geometry of the coolant flow channels, and with it the associated temperature distribution in the flow channels. Finally, this new temperature distribution about the fuel elements replaces the initial nominal temperature environment. Since the solution to this problem requires determination of the steady-state relationship between all fuel element force deflection responses and the temperature distribution in all coolant flow channels, an approach involving iterations is strongly suggested. Shown in Figure 1 is a cross section through the fuel element array considered, including the numbering convention for fuel elements, coolant channels and nomenclature. To attenuate the effect of artificial boundary conditions upon the primary elements, a zone of secondary elements has been included as indicated. The final results are assumed to be valid for primary elements, while results for the secondary elements could be distorted by the adjacent boundary elements.

The study of the problem begins by considering any one fuel element (tube) of the bundle and its characterizing inter-relationships between temperature distribution along the shell, mode shape, and external restraining forces or moment. By removing the

mechanical constraints, the element assumes its unrestrained ("free-bow") mode shape, given by its thermal deflection plus its initial manufacturing bow, if any. In the approach described, the tube cross-sectional geometry is limited to cylindrical shells of circular, quasi-circular, and polygonal cross-sectional shapes. The subsequent derivations follow closely circular cross sections, but can readily be adapted to the other kinds of cross-sectional geometries indicated.

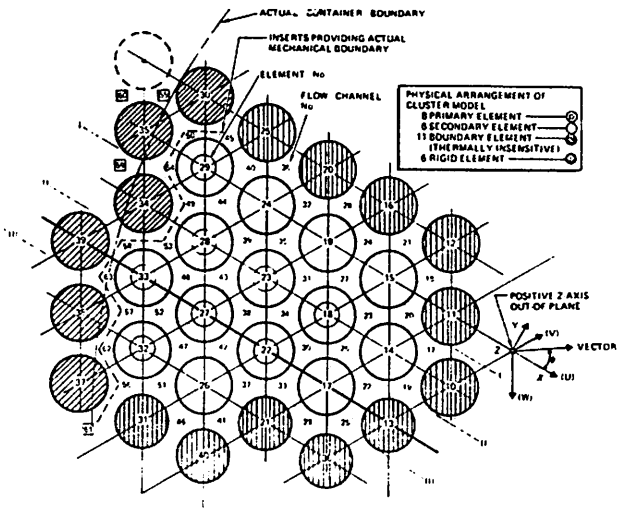

Figure 1. Physical Arrangement of Cluster Model

II. UNRESTRAINED MODE SHAPE

A. Determine Equivalent Thermal Gradient

Shown in Figure 2a is a developed view of the tube shell, together with the grid system defining the initial temperature input points. Shown in Figure 2b is a view of any one of the shell strips of Figure 2a, with an indication of a typical temperature distribution and associated variations in length for the fibres of the shell strip. The immediate object of this development is a determination of the thermally induced "free-bow" shape for each shell increment of Figure 2a. Applied to each of these shells are the conditions of equilibrium for zero-resulting axial force and zero-resulting gross bending moment.

The force, dF, to be applied to each shell fibre to compress or extend it to the mean fibre length, $\Delta\bar{L}$, is

$$dF = \bar{\alpha} E R t (\bar{T} - T_\theta) \, d\theta \, (lb) \quad , \tag{1}$$

wherein the mean fibre temperature, $\bar{T}$, is

$$\bar{T} = \frac{1}{2\pi} \int_{\theta=0}^{2\pi} T_\theta \, d\theta \quad (°F). \tag{2}$$

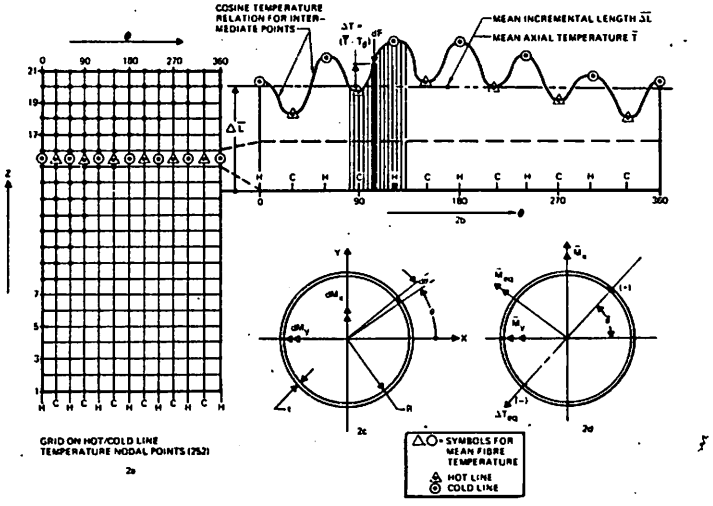

Figure 2. Determination of Equivalent Thermal Gradient

The incremental moments $d\bar{M}$, dM_x, dM_y associated with each incremental force, dF, are:

$$d\bar{M} = R\, dF_\theta \quad , \tag{3a}$$

$$dM_x = R \cos\theta \; dF_\theta \quad , \tag{3b}$$

$$dM_y = R \sin\theta \; dF_\theta \quad . \tag{3c}$$

Integrating to obtain resultant moments

$$\bar{M}_x = tR^2 \bar{\alpha} E \int_0^{2\pi} \cos\theta \, (\bar{T} - T_\theta) \, d\theta \quad , \tag{4a}$$

$$\bar{M}_y = tR^2 \bar{\alpha} E \int_0^{2\pi} \sin\theta \, (\bar{T} - T_\theta) \, d\theta \quad , \tag{4b}$$

$$\bar{M}_{eq} = \sqrt{\bar{M}_x^{\,2} + \bar{M}_y^{\,2}}$$

$$= tR^2 \bar{\alpha} E \sqrt{\left[\int_0^{2\pi} \sin\theta \, (T - T_\theta) \, d\theta\right]^2 + \left[\int_0^{2\pi} \cos\theta \, (T - T_\theta) \, d\theta\right]^2} \quad , \tag{4c}$$

and the orientation of the equivalent moment, $\bar{M}_{eq}$, is

$$\theta = \tan^{-1}\left(\frac{\bar{M}_y}{\bar{M}_x}\right) .$$

The equivalent temperature gradient, $\overline{\Delta T}_{eq}$, for a tube increment is defined as the diametral linear temperature gradient causing a rotation, $\bar{\phi}$, of the end faces of the length increment, identical in magnitude to the rotation obtained by relieving the moment, $\bar{M}_{eq}$. From this

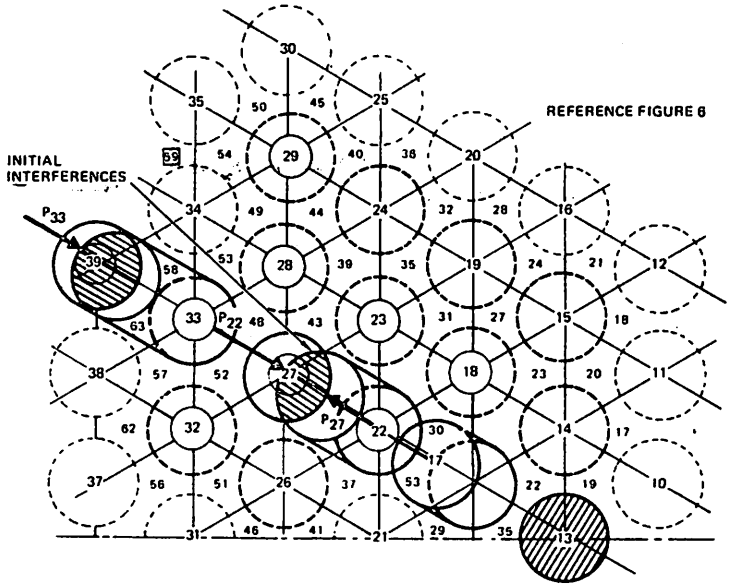

Figure 4. Sequential Progress of Assembling Increments

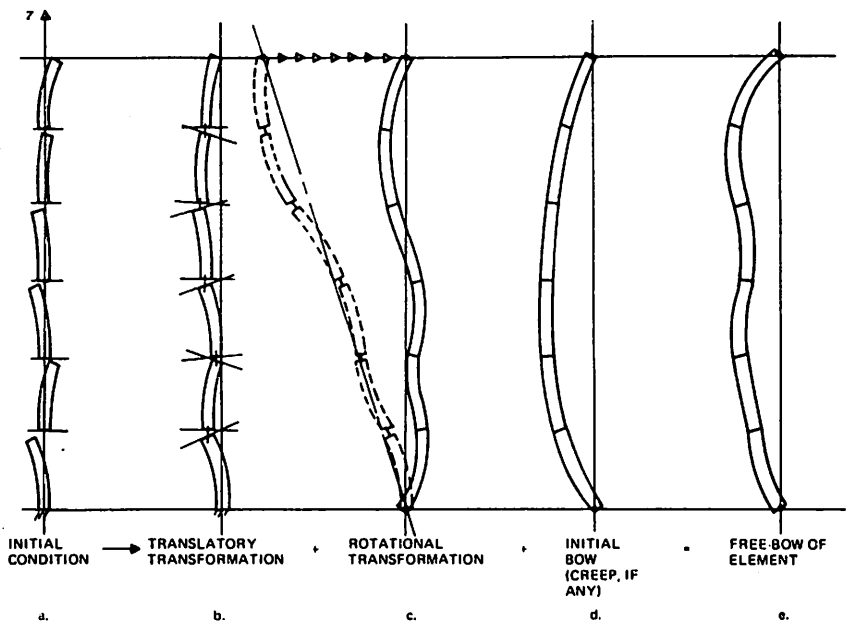

Figure 5. Typical Initial Free Bow Interference

studied is of a discontinuous nature, and has a potentially large number of primary variables (i. e., contact forces), it is doubtful whether these prerequisites could be established on a practical basis. This method was therefore dropped for lack of promise.

2. Matrix Approach

This candidate approach is based on establishing a mathematical relationship between all magnitudes of interference and all associated contact forces. In reality, this route would necessitate a system of linear equations whose order would be equal to the sum total of all possible contact forces, or about of order 75 for the physical model described previously. A significant complication in this approach stems from the fact that the system is essentially nonlinear (i. e., at points of potential interference, the contact force is equal to zero, rather than negative, if a clearance exists). The foregoing, together with considerable uncertainties regarding the inversion of the attendant large matrix of influence coefficients and the probable compounding of these types of problems, should a considerably larger cluster pattern be desired at some later time, were the reasons for bypassing this potential solution approach at present.

3. Interactive Method

This method involves a quite simple mathematical model describing the interaction of two adjacent fuel elements. If any element is in contact with several polarly adjacent elements, this model effectively decouples interference effects lying in either of the other two main planes. On this basis, the task of obtaining mechanical inter-element compatibility is greatly simplified, by successively studying only single rows of the fuel element cluster. This approach, in general, leads to the creation of new (smaller) interferences between the in-plane elements and adjacent elements lying in one of the other main planes. This cause-and-effect relationship, then, illustrates the nature of the iteractive method followed in obtaining inter-element compatibility for the cluster studied. The interative method was chosen as the preferred approach, due to its great lucidity in operation and suitability, in view of a possible later expansion of the cluster size. A brief explanation of how this method works follows.

C. DETERMINE INTER-ELEMENT COMPATIBILITY

Shown in Figure 6 is a typical section along a row of elements in the cluster (indicated by ——————— in Figure 1) (Also see Figure 5). In general, a row of elements starts with a thermally insensitive boundary element, is followed by several active elements, and ends with a rigid element representing the external containment boundary. Shown in Figure 6 is a possible relationship of initial (unrestrained) lateral deformations for a row of elements. The magnitudes of deformation indicated represent, of course, only the in-plane component of the initial 3-dimensional free-bow shape for any element. The cluster considered is composed of fifteen such rows, each containing six elements (sometimes including one or two dummy elements at its end). The computer routine has been designed to calculate the clearance or interference between any adjacent elements at a prespecified distance from the element support points (e. g., at axial nodal Point No. 12, as shown). For a general element support condition (i. e., a moment at each end and an intermediate lateral force) the rotations and deflection produced by these effects at these points may be expressed as follows:

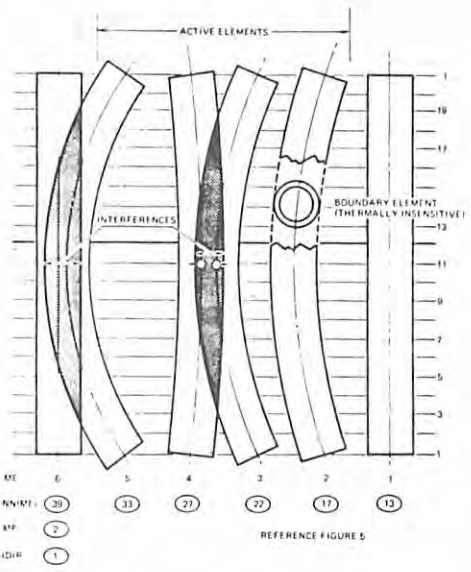

Figure 6. "Free-Bow" Interference in Typical Row of Elements

$$\begin{bmatrix} \theta_1 \\ \delta_2 \\ \theta_3 \end{bmatrix} = \begin{bmatrix} a_{11} & a_{12} & a_{13} \\ a_{21} & a_{22} & a_{23} \\ a_{31} & a_{32} & a_{33} \end{bmatrix} \bullet \begin{bmatrix} M_1 \\ P_2 \\ M_3 \end{bmatrix} , \tag{11}$$

where a_{ij}'s represent the structural flexibility constants of the structural system. For a system with simply supported elements, the force deflection relationship is

$$\delta_2 = a_{22} P_2 = \frac{L^3}{48EI} P_2 . \tag{12}$$

If an interference is indicated, the program calculates a force to be applied between the two respective elements, reducing the magnitude of their interference to a small valve. After scanning all possible rows of elements, the force components for each element are converted into an equivalent single force of given magnitude and direction. From this, the associated corrective beam deflection is calculated for each element, and superposed upon its initial free-bow deflection. The resulting new deflection distribution for the elements gives rise to the next round of mechanical iteration, determining a new set of interference conditions, a new set of interference forces (to be superposed upon the existing set of forces), and a new element deflection distribution, etc.

Upon achieving satisfactory interelement compatibility (i.e., near zero interferences at points of contact forces), the mechanical iteration routine is terminated, and the program advances into its thermal routine.

IV. THERMAL BEHAVIOR OF CLUSTER

A. GENERAL

The ideal structural behavior of a reactor core, including fuel elements and associated restraining suspension system, is characterized by the achievement of decoupling between thermal and mechanical interactive effects. Since conventional structural reactor materials display a rather high thermal expansiveness, and since restraining systems to counteract such thermal deformations often are neither practical nor effective, reactor internal deflections and forces of thermal origin frequently become the governing mechanical design considerations.

A typical problem in this area involves the effect of lateral fuel element deformations upon the temperature distribution along coolant channels bounded by these elements. This mechanical-thermal cause-and-effect relationship becomes, generally, more pronounced as the ratio of lateral fuel element pitch to cladding outer diameter approaches unity. For the problem considered, the fuel elements are clustered tightly, with the P/D ratio near unity (1.02 to 1.05).

The problem indicated commands special attention, since the factors controlling it have a "vicious circle" interrelationship. Therefore, a meaningful solution to the problem studied must yield a steady-state relationship for the interacting parameters. A more detailed description of the problem of thermal-mechanical behavior amongst adjacent fuel elements follows.

B. THERMAL-MECHANICAL INTER-ELEMENT BEHAVIOR

Considered subsequently is an array of fuel elements with pinned - pinned end conditions, and an arbitrary length for the fuel elements. This beam model can be shown to produce more severe thermal-mechanical element interactions than a model with full or partial end fixity at one end of the fuel element. Depicted in Figure 7 is a possible sequence of element deflection responses to a given nominal temperature distribution for the coolant channels. Shown in Figure 7a is a highly idealistic case, characterized by uniform coolant channel temperatures in the radial direction. Consequently, the ideal geometry of the array, and with it the coolant channel cross sections, remain unaffected. Shown in Figure 7b is a case with a non-uniform (i. e., optimized) coolant temperature distribution. Indicated therein is the possible lateral displacement response of the elements to the given temperature condition. A net effect of a nonuniform temperature distribution (assumed to be independent of θ) is, in general, an increase or a decrease of flow area for each coolant channel. For illustrative purposes, a possible lateral displacement response of the elements is indicated in Figure 7b. Indicated therein are coolant flow channels, expected to reduce or increase their flow area, thereby increasing or decreasing their nominal channel temperature. Plotting the new flow channel temperature over the radial core coordinate (see Figure 7c) suggests that initial nominal radial temperature gradients may become steeper, due to the clustering effects within the array. Since the initial mechanical response of the fuel elements tends to modify the initial channel temperatures, a new mechanical response of the fuel elements needs to be determined, based on the modified temperature distribution. This sequence, interactive in nature, stops once the fuel elements have achieved a stable cluster pattern (i. e., one in which, during subsequent iterations, the flow channel cross sections

remain essentially unchanged).

C. COMPUTATIONAL APPROACH

The next step toward obtaining a solution for the problem studied requires determination of the modified flow-channel temperatures, and from these the new cladding temperatures. Thereafter, the iterative process may begin a new cycle.

1. Calculate Modified Flow Channel Areas and Temperatures

This task builds upon the results of the mechanical iteration phase. Therein, the lateral 3-dimensional deflection shape of each element was determined, so as to achieve mechanical inter-element compatibility consistent with a given temperature distribution. However, during the mechanical iteration phase, the flow channel areas, in general, changed, but the underlying temperature distribution was assumed to remain undisturbed. During the thermal iteration phase, an essentially inverse assumption is made (i.e., new temperatures are calculated, assuming mechanical invariance).

The method to calculate new flow channel cross sections uses a very general approach, as indicated in Figure 8. The nominal flow channel area, A_{nom}, is calculated from the outer diameter, D, of the fuel elements and the pitch, P, between the fuel elements. The new flow channel area, A_{new}, is determined by adding and subtracting differential flow areas (DFA) Δ's, as indicated in Figure 8. As an example, the DFA $\Delta 1$ and $\Delta 2$ are calculated from the element displacement vector, V_1, and its associated orientation, θ_1 (cf. results of the mechanical iteration), thus:

$$\Delta_1 = \frac{PV_1}{2} \sin (\theta_1 + 60) \quad , \tag{13}$$

$$\Delta_2 = \frac{PV_1}{2} \sin (\theta_1) \quad . \tag{14}$$

In general, six such DFA Δ's are calculated to yield the new local flow channel cross section, thus:

$$A_{new} = A_{nom} + \sum_{i=1}^{6} \Delta_i \quad . \tag{15}$$

The new flow-channel temperature is derived from the following semi-empirical equation

$$\Delta T_{new} = m \Delta T_{nom} \left(\frac{A_{nom}}{A_{new}} \right)^n \quad . \tag{16}$$

Eq. 16 gives the rise in flow-channel temperature, ΔT_{new}, along an axial channel increment. The determining variables are:

ΔT_{nom} = nominal (ideal) channel temperature rise along an increment having a channel of nominal cross section, A_{nom}

A_{new} = new channel flow area

n = empirical factor, allowing for variations in flow-related variables (representative value $\simeq$ 1.67)

m = empirical mixing factor which considers the effect of inter-channel coolant

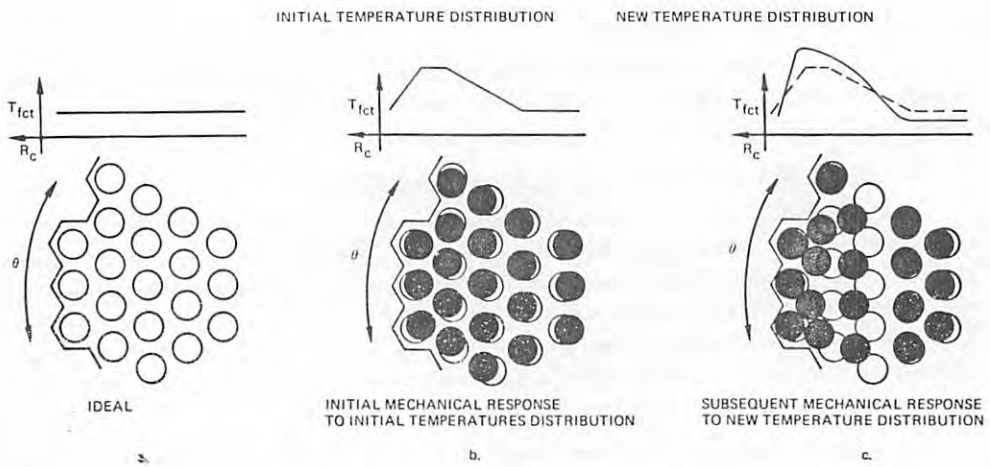

Figure 7. Thermal-Mechanical Element Interactions

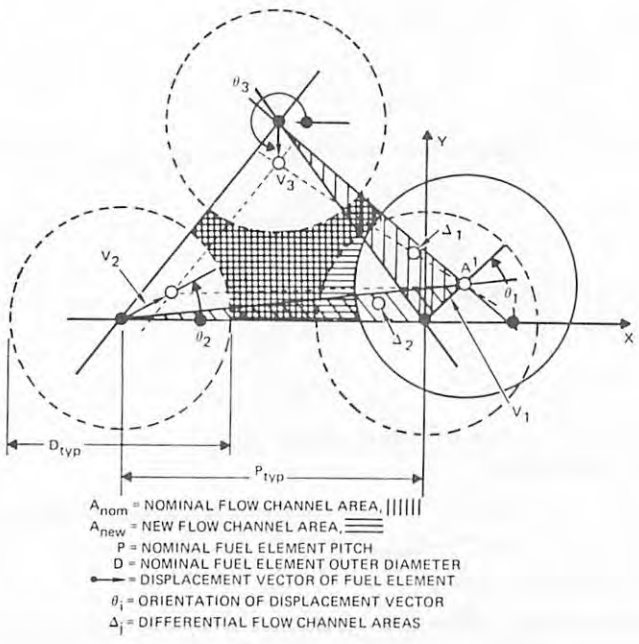

Figure 8. Coolant Flow Channel Geometry

mixing (representative value $\simeq 0.70$).

A general expression for the new temperature distribution in a flow channel is

$$T_{i_{new}} = T_o + m \sum_{i}^{j} \left[\Delta T_{nom_j} \left(\frac{A_{nom}}{A_{new}} \right)_j^n \right] (°F) \quad , \tag{17}$$

wherein T_o = base or reactor inlet temperature.

The last step remaining before a new round of iteration may begin involves calculating a new temperature distribution for each fuel element cladding. The basic approach to this step is similar to the method employed for the calculation of channel temperatures (i. e., the nominal temperature data, initially derived from a refined thermal analyser program, is adjusted for the effects of changes in flow channel area, cf eq. 13 to 15, and associated new temperatures in the flow channels, cf eq. 17). Variation of the temperature, $U_{j,k}$, at a cladding surface point (j, k) is assumed to be proportionate to the variation in temperature of adjacent flow channels. The general expression for the temperature $U_{j,k}$ is, if k = even (see Figure 9):

$$U_{new_{j,k}} = U_{nom_{j,k}} + \left(FCHT_{new_j} - FCHT_{nom_j} \right)_k (°F) \quad . \tag{18}$$

If k = odd:

$$U_{new_{j,k}} = U_{nom_{j,k}} + \frac{1}{2} \left\{ \left(FCHT_{new_j} - FCHT_{nom_j} \right)_k + \left[FCHT_{new_{(j+1)}} - FCHT_{nom_{(j+1)}} \right]_k \right\} (°F) \quad . \tag{19}$$

These simple calculations are believed to be sufficiently accurate, if no large changes (e. g., $\gtrsim$30%) in flow-channel areas are involved, and if the initial (nominal) temperature data was derived by an accurate and representative thermal model. Otherwise, the new flow channel and new cladding temperature data should be calculated by a thermal analysis program, based on the new coolant channel cross sections as developed by the mechanical iteration phase (cf eq. 15).

V. EXAMPLE AND RESULTS

A. GENERAL

A sample problem, processed through the detail steps of the approach outlined, is briefly described here. The results are given only as they pertain to the primary fuel elements (i. e., Element No. 18, 22, 23, 27, 28, 29, 32, and 33). Results pertaining to the secondary element have been generated as well, but are not given, since they may be influenced by the close proximity to elements with artificial boundary conditions. The initial temperature distribution for each of the flow channels affecting primary elements is given in Table I.

Figure 10 shows plots of those initial coolant channel temperatures, which approximately lie in one of three parallel and nearly radial planes (see Planes I, II, and III in Figure 1). Shown in Table II is the initial cladding temperature distribution for Element No.27. For brevity, similar data, generated for the other primary elements, is not included.

TABLE I

INITIAL FLOW CHANNEL TEMPERATURES AFFECTING PRIMARY ELEMENTS (°F)

	Z/L	0.	.10	.20	.30	.40	.50	.60	.70	.80	.90	1.00
	NODAL NO.	1	3	5	7	9	11	13	15	17	19	21
F	23	1065.0	1072.5	1072.7	1088.1	1108.2	1135.1	1145.3	1155.2	1173.7	1186.9	1194.4
L	26	1065.0	1073.8	1074.0	1090.2	1111.0	1138.3	1148.6	1158.4	1176.7	11.89.7	1196.4
O	27	1065.0	1073.6	1073.8	1089.7	1111.0	1136.7	1146.7	1156.3	1174.2	1186.8	1193.4
W	30	1065.0	1075.0	1075.3	1094.2	1118.4	1150.2	1161.9	1173.2	1194.2	1208.9	1216.3
	31	1065.0	1074.9	1075.1	1093.8	1117.7	1149.1	1160.7	1171.9	1192.6	1207.1	1214.5
C	33	1065.0	1074.9	1075.2	1094.2	1118.9	1151.7	1164.0	1176.8	1197.7	1213.1	1221.1
H	34	1065.0	1074.8	1075.1	1093.8	1118.1	1150.4	1162.6	1174.4	1196.3	1211.8	1220.1
A	35	1065.0	1074.7	1074.9	1093.5	1117.7	1149.8	1161.9	1173.5	1195.0	1210.2	1218.2
N	37	1065.0	1074.6	1074.9	1093.3	1117.3	1149.6	1161.8	1173.6	1195.6	1211.3	1219.9
N	38	1065.0	1074.6	1074.8	1093.0	1116.8	1148.6	1160.7	1172.4	1194.3	1209.9	1218.6
E	39	1065.0	1074.5	1074.7	1092.9	1116.6	1148.4	1160.5	1172.2	1194.1	1209.6	1218.3
L	42	1065.0	1074.4	1074.7	1092.8	1116.5	1148.4	1160.5	1172.3	1194.3	1210.0	1218.8
	43	1065.0	1074.4	1074.7	1092.7	1116.2	1147.9	1159.9	1171.5	1193.4	1208.9	1217.7
	44	1065.0	1074.5	1074.8	1092.9	1116.5	1143.3	1160.3	1171.9	1192.7	1209.3	1213.0
	45	1065.0	1074.7	1075.0	1092.1	1116.8	1148.5	1160.5	1172.1	1193.8	1209.4	1218.0
I.	47	1065.0	1074.4	1074.7	1092.7	1116.3	1148.0	1160.1	1171.8	1193.8	1209.4	1218.3
D.	48	1065.0	1074.7	1074.9	1093.1	1117.0	1148.9	1161.1	1172.8	1194.8	1210.5	1219.3
No.	49	1065.0	1074.8	1075.0	1093.3	1117.2	1149.0	1160.9	1172.5	1194.2	1209.8	1218.3
	50	1065.0	1073.8	1074.0	1091.4	1114.0	1144.6	1156.3	1167.6	1188.8	1204.2	1213.1
	51	1065.0	1074.5	1074.8	1092.8	1116.4	1148.0	1160.0	1171.7	1193.5	1209.1	1217.8
	52	1065.0	1074.8	1075.0	1093.6	1117.9	1150.4	1162.7	1174.5	1196.7	1212.5	1221.2
	53	1065.0	1075.1	1075.3	1094.0	1118.4	1150.8	1163.0	1174.8	1196.9	1212.8	1221.4
	54	1065.0	1073.8	1074.0	1091.1	1113.4	1143.3	1154.6	1165.6	1186.4	1201.7	1210.4
	56	1065.0	1074.9	1075.1	1093.8	1117.9	1150.2	1162.3	1173.9	1195.9	1211.8	1220.5
	57	1065.0	1075.3	1075.5	1094.4	1118.8	1151.2	1163.3	1174.9	1196.8	1212.7	1221.1
	58	1065.0	1074.3	1074.5	1092.8	1116.5	1148.3	1160.3	1172.0	1193.9	1210.0	1219.0
	62	1065.0	1073.8	1074.0	1091.7	1114.9	1146.0	1157.9	1169.4	1191.0	1207.0	1216.2
	63	1065.0	1074.3	1074.5	1092.6	1116.0	1147.4	1159.2	1170.7	1192.3	1208.3	1217.3

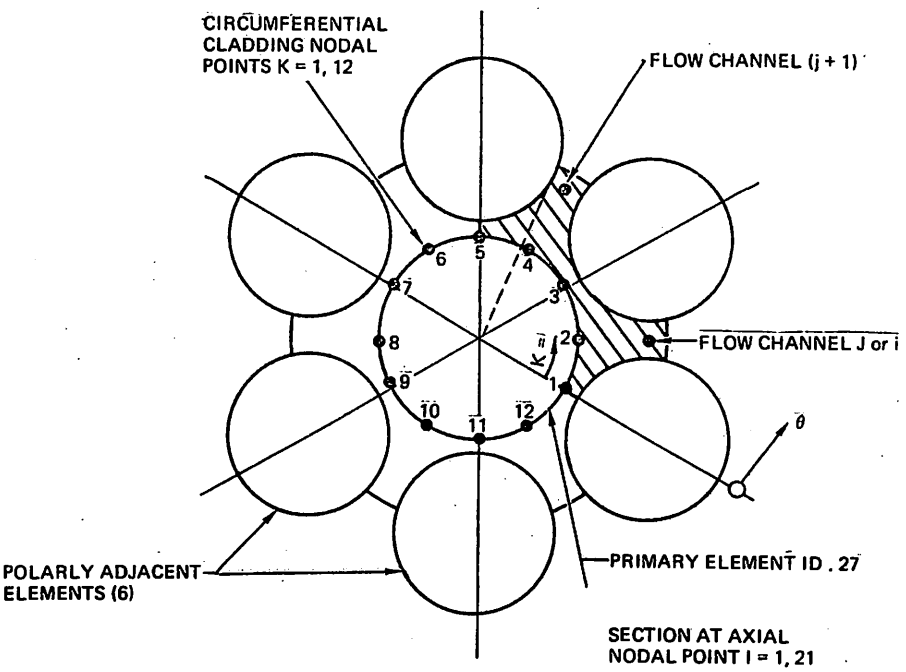

Figure 9. Determination of Cladding Temperature

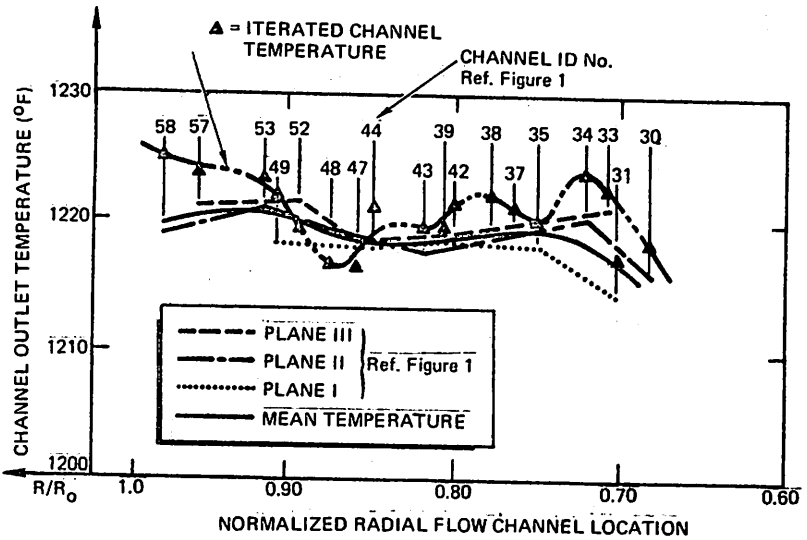

Figure 10. Iteration Effect on Channel Outlet Temperatures

TABLE II

INITIAL CLADDING (MEAN) SURFACE TEMPERATURE DISTRIBUTION FOR ELEMENT No. 27

		CIRCUMFERENTIAL NODAL POINTS AT 30° INTERVALS												
		Z/L	1	2	3	4	5	6	7	8	9	10	11	12
AXIAL NODAL POINTS	1	0.00	1068.3	1065.0	1068.3	2065.0	1068.3	1065.0	1068.3	1065.0	1068.3	1065.0	1068.3	1065.0
	2	0.05	1076.7	1069.8	1076.7	1069.7	1076.7	1069.8	1076.8	1069.9	1076.8	1069.7	1076.7	1069.7
	3	0.10	1085.1	1074.6	1085.1	1074.4	1085.1	1074.7	1085.3	1074.8	1085.2	1074.4	1085.0	1074.4
	4	0.15	1085.3	1074.7	1085.3	1074.5	1085.4	1074.8	1085.6	1074.9	1085.5	1074.5	1085.3	1074.5
	5	0.20	1085.6	1074.8	1085.6	1074.7	1085.6	1074.9	1085.8	1075.0	1085.7	1074.7	1085.6	1074.7
	6	0.25	1095.6	1083.9	1095.6	1083.7	1095.7	1084.0	1096.2	1084.3	1095.9	1083.7	1095.5	1083.7
	7	0.30	1105.5	1093.0	1105.5	1092.7	1105.8	1093.1	1106.5	1093.6	1106.2	1092.7	1105.5	1092.8
	8	0.35	1118.7	1104.9	1118.7	1104.4	1119.0	1105.0	1119.9	1105.7	1119.5	1104.5	1118.6	1104.7
	9	0.40	1131.9	1116.8	1131.8	1116.2	1132.2	1117.0	1133.3	1117.9	1132.8	1116.3	1131.8	1116.5
	10	0.45	1148.1	1132.7	1148.0	1132.0	1148.4	1132.9	1149.7	1134.1	1149.1	1132.1	1148.0	1132.5
	11	0.50	1164.3	1148.6	1164.1	1147.9	1164.6	1148.9	1166.1	1150.4	1165.5	1148.0	1164.2	1148.4
	12	0.55	1170.0	1154.7	1169.8	1153.9	1170.3	1155.0	1171.9	1156.5	1171.3	1154.1	1169.9	1154.5
	13	0.60	1175.7	1160.7	1175.5	1159.9	1176.0	1161.1	1177.7	1162.7	1177.1	1160.1	1175.6	1160.5
	14	0.65	1181.2	1166.6	1181.0	1165.7	1181.6	1166.9	1183.3	1168.6	1182.6	1166.0	1181.2	1166.4
	15	0.70	1186.8	1172.4	1186.5	1171.5	1187.1	1172.8	1188.8	1174.5	1188.2	1171.8	1186.7	1172.3
	16	0.75	1196.21	1183.4	1195.9	1182.5	1196.4	1183.8	1198.1	1185.6	1197.5	1182.8	1196.1	1183.3
	17	0.80	1205.6	1194.3	1205.3	1193.4	1205.7	1194.8	1207.4	1196.7	1206.8	1193.8	1205.5	1194.3
	18	0.85	1212.3	1202.1	1211.9	1201.2	1212.3	1202.6	1213.9	1204.6	1213.4	1201.6	1212.1	1202.1
	19	0.90	1218.9	1209.9	1218.5	1208.9	1218.8	1210.5	1220.5	1212.5	1219.9	1209.4	1218.7	1210.0
	20	0.95	1220.3	1214.3	1219.8	1213.3	1220.2	1214.9	1221.8	1216.9	1221.3	1213.9	1220.1	1214.4
	21	1.00	1221.6	1218.6	1221.2	1217.7	1221.5	1219.3	1223.1	1221.2	1222.6	1218.3	1221.5	1218.8

B. FREE-BOW SHAPE OF ELEMENT

A task, preliminary to the definition of the free-bow shape of an element, is the determination of the equivalent gross bow temperature gradient for each incremental length of the element. These gradients have been calculated, by the subroutine "SIXPHX" of the main program "SAS3D," for all active elements. These data, as applicable to Element No. 27, are given in Table III. The basis for these results is the initial cladding surface temperature distribution for the Element No. 27, as given by Table II.

TABLE III
EQUIVALENT INITIAL GROSS BOW THERMAL GRADIENTS FOR ELEMENTS NO. 27

	INCREMENT NUMBER																			
	1	2	3	4	5	6	7	8	9	10	11	12	13	14	15	16	17	18	19	20
ΔT_{eq}(°F)	0.06	0.18	0.24	0.24	0.37	0.64	0.87	1.05	1.27	1.50	1.66	1.74	1.81	1.85	1.88	1.88	1.88	1.85	1.85	1.86
ϕ_{eq}(°)	3.5	4.0	4.0	3.5	7.0	9.0	11.5	13.0	15.5	17.5	19.0	20.0	21.0	22.0	23.5	25.5	26.5	27.5	29.0	30.5

NOTE: ϕ_{eq} IS MEASURED FROM POSITION X-AXIS COUNTERCLOCKWISE TO "COLDEST" FIBRE OF SHELL INCREMENT

Progressing to the subroutine "SNAKEX" of the main program, the equivalent temperature gradients become the basis for determining the attendant bowing deformation of each increment of an element. The same subroutine also "assembles" these deformed increments into a continuous beam with simply supported end conditions. If desired, a restraining moment, corresponding to full fixity at one end of the beam, may be determined, and the associated 3-dimensional beam mode shape is calculated for either type of end fixity. The free-bow deflection for Element No. 27 with pinned ends due to the thermal loads, per Table III, is shown in Figure 11. The "free" element shape, as shown in Figure 11, does not yet include the initial manufacturing bow characteristics, if any. However, these, as well as possible creep bow effects accrued, may be superimposed upon the element's "free-bow" shape at this point, and before the study of element interaction begins.

C. ELEMENT INTER-ACTIVE EFFECTS

1. Mechanical

Upon determining the "free-bow" shape of each active element (see Section II), they are placed in the appropriate location of the element array. Considering discreet element deflections at the force plane (assumed to be located at Z/L = 0.60) yields a comprehensive view of the task of achieving inter-element compatibility.

Entering the subroutine "FORCEX" for a predetermined number of mechanical compatibility iterations yields a characteristic cluster pattern and force conditions, shown in Figure 12, with each of the elements having its deflection shape fully defined over its entire length.

2. Thermal

In the thermal iteration subroutine "THERMX," new flow channel areas and temperatures are calculated, based on the geometries determined by the last mechanical iteration phase. The result by "THERMX" is a new temperature distribution for the fuel element cladding, superseding the initial conditions (see Tables I and II). However, a considerably more practical way to appraise the thermal iteration effects is a comparison of new vs

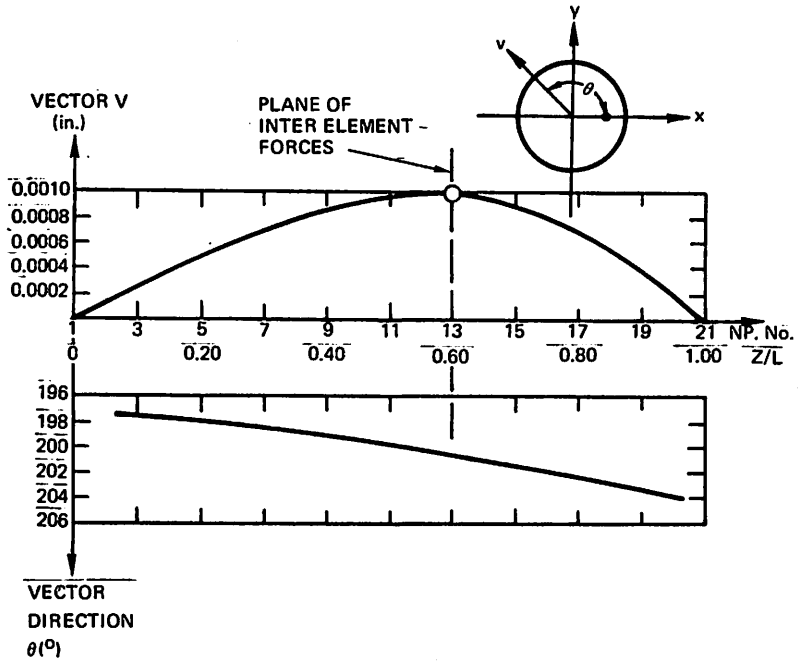

Figure 11. "Free-Bow" Shape, Element No. 27 (Pinned Ends)

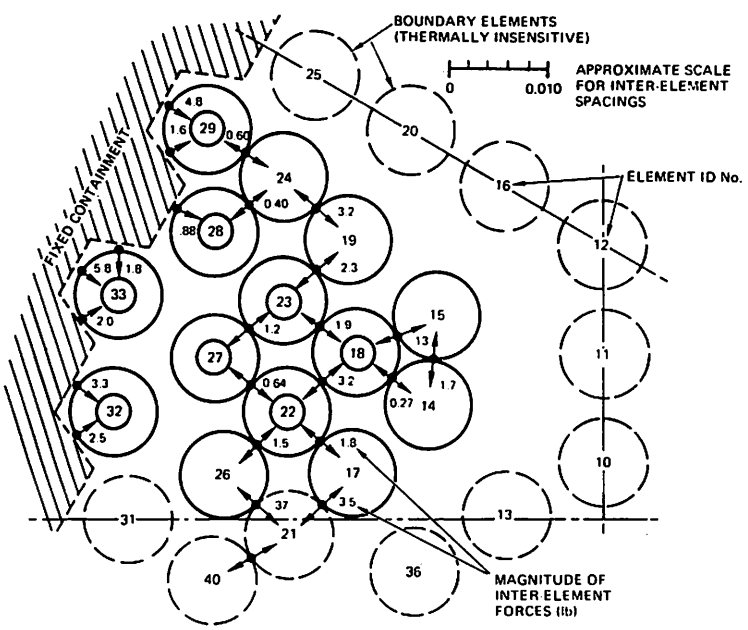

Figure 12. Cluster Pattern and Force Levels

previous gross bow temperature gradients. Of course, each pass through the thermal section of the program is accompanied by several (e.g., 4 to 8) passes through the mechanical iteration loop. At this stage, the main objective of the calculational effort is to find a steady-state relationship between the mechanical (forces, clearances, flow areas, and interference) and the thermal (temperature of flow channels, cladding surface, and gross bow gradients) parameters. To aid in assessing the respective degree of accomplishment, the results at the end of each thermal iteration, including the resulting gross bow gradients, have been compared, and show good convergence (see Table IV).

TABLE IV

EFFECT AND RESULTS OF ITERATIVE PROCESS

Element Identification Number	Initial "Free" Condition	Thermal Iteration Cycle 1		Thermal Iteration Cycle 2		Thermal Iteration Cycle 3		Thermal Iteration Cycle 4	
		Number of Mechanical Iterations Within Thermal Iteration Cycle: 5		6		7		9	
		Net Element Forces and Their Directions							
		Force (lb)	∢Force (°)	Force (lb)	∢Force (°)	Force (lb)	∢Force (°)	Force (lb)	∢Force (°)
18		4.09	35.3	4.14	38.9	4.11	40.5	4.14	39.5
22		2.81	210.0	2.44	207.9	2.49	214.2	2.49	215.7
23		2.85	203.2	2.45	178.65	2.51	201.9	2.67	201.0
27		0.18	240.0	1.65	223.7	1.62	220.9	1.62	220.1
28		0.19	360.0	0.68	355.7	0.72	370.7	0.76	331.5
29		4.20	0.30	5.82	6.7	5.46	7.4	5.54	7.1
32		3.28	22.2	5.32	26.5	5.09	25.6	5.03	25.1
33		5.61	1.82	8.08	359.7	7.73	0.96	7.72	1.09
		Equivalent (Peak) Bow Gradient (°F)							
18		27.4		28.3		28.2		28.0	
22		2.49		1.48		1.42		1.43	
23		1.78		2.71		2.56		3.01	
27		1.92		3.50		4.31		4.29	
28		3.14		4.50		4.57		4.89	
29		14.0		18.3		17.2		17.4	
32		11.2		16.9		16.4		16.2	
33		17.3		24.0		23.0		23.0	

VI. SUMMARY

The approach presented shows good convergence characteristics for both mechanical and thermal iterations. The results show that elements with relatively low gross bow gradients may still be subjected to relatively high contact forces by neighboring elements, and vice versa. Clustering effects were observed to considerably modify the local initial thermal environment. Upon incorporating bending creep effect capability, the approach described permits the study of the time-dependence of the cluster pattern under steady-state operating conditions, as well as the effects of thermal shocks.

The method described may also be utilized for other applications (e. g., for certain types of heat exchangers, boilers, etc.).

The preceding results assume initially perfectly straight elements, and are based on the following material and structural input constants:

Description	Symbol	Value
Youngs Modules	E	22×10^6 psi
Coefficient Thermal Expansion Thermal Expansion	$\bar{\alpha}$	11.2×10^{-6} in. /in. -°F
Moment of Inertia	$(\pi R^3 t)$	0.003531 $in.^4$
Nominal Inter-Element Clearance	SNOM	0.002 in.
Element Support Spacing	L	18.5 in.
Location of Force Plane at	Z/L	0.60

DISCUSSION

Q R. A. VALENTIN, U. S. A.

What are the computer time requirements of typical program applications ? Are there any convergence problems ? Has the program ever been used in LMFBR case ? Could you elaborate on the mixing assumptions used in the program ?

A A. J. BAUMGARTNER, U. S. A.

Computer (= central processor) time required for the sample problem shown is about 35 minutes for IBM-360/36 or about 5 minutes for IBM-360/85 system. No significant convergence problems in either the thermal or the mechanical processing area have been encountered. (Ref. Table IV). At present the program has not been used for a specific LMFBR - application. Mixing effects are reflected in the initial thermal input to the program. These input data are generated by a relatively sophisticated thermal analyser program focusing strongly on mixing effects. However, in the course of the thermal iteration procedure, a simpler model is used to correlate flow channel area changes with attendant flow channel temperature changes. Therein, and for small ranges of iterative change in the flow areas (Ref. answer to Dr. Wolf's question) mixing effects are considered to be invariant.

Q L. WOLF, Germany

Do you take account for variations in velocity distributions and eddy diffusivity distributions for heat and momentum in your iterative procedure ?

A A. J. BAUMGARTNER, U. S. A.

In its present form the thermal iteration procedure does not take account for the effects you mention. Since the program is designed for tightly clustered arrays, variations between initial and final flow channel areas have been verified to be minor ($\lesssim 10\%$) and, therefore, are not expected to result in significant variations of magnitudes for the parameters in question. However, for significant changes in flow channel areas (e. g., $\lesssim 30\%$) the current thermal iteration approach should be replaced by a more sophisticated thermal analysis program.